International Journal of Heat and Mass Transfer 117 (2018) 1368–1383

Contents lists available at ScienceDirect

International Journal of Heat and Mass Transfer

journal homepage: www.elsevier.com/locate/ijhmt

Review

Pool boiling critical heat flux (CHF) – Part 2: Assessment of models and correlations

Gangtao Liang [a,b], Issam Mudawar [b,*]

[a] Key Laboratory of Ocean Energy Utilization and Energy Conservation of Ministry of Education, School of Energy and Power Engineering, Dalian University of Technology, Dalian 116024, China

[b] Purdue University Boiling and Two-Phase Flow Laboratory (PU-BTPFL), School of Mechanical Engineering, 585 Purdue Mall, West Lafayette, IN 47907, USA

ARTICLE INFO

Article history:
Received 12 July 2017
Received in revised form 14 September 2017
Accepted 18 September 2017
Available online 28 September 2017

Keywords:
Pool boiling
Critical heat flux (CHF)
Orientation effects
Contact angle

ABSTRACT

This paper is the second part of a two-part study on pool boiling critical heat flux (CHF) from flat surfaces. While the first part reviewed different CHF models and associated mechanisms and parametric trends, the present part is dedicated to the assessment of both models and correlations. The assessment is based on a new consolidated CHF database consisting of 800 data points amassed from 37 sources, and includes 14 working fluids, pressures from 0.0016 to 5.2 MPa, orientation angles from 0 to 180°, and contact angles from 0 to 113°. It is shown that a modified hydrodynamic instability model and the interfacial lift-off model provide the best predictions for CHF from horizontal, upward-facing surfaces. Modified with a correlation for surface orientation effects, the same models also provide the best predictions for inclined surfaces. However, all models and correlations lose accuracy at or near the downward-facing orientation, which points to the need for more data and improved understanding of near-wall interfacial behavior for these orientations. Finally, recommendations are provided for prediction of contact angle effects.

Contents

1. Introduction

Recent performance advances in applications such as high-performance computers, electrical vehicle power electronics, avionics, and directed energy laser and microwave weapon systems, have led to unprecedented increases in power density. With

* Corresponding author.
E-mail address: mudawar@ecn.purdue.edu (I. Mudawar).
URL: https://engineering.purdue.edu/BTPFL (I. Mudawar).

https://doi.org/10.1016/j.ijheatmasstransfer.2017.09.073
0017-9310/

Nomenclature

A	area
c_p	specific heat at constant pressure
g	gravitational acceleration
H	wall thickness
h_{fg}	latent heat of vaporization
k	thermal conductivity; coefficient
P	pressure
P_c	critical pressure
Pr	Prandtl number
q''_{CHF}	critical heat flux
R_i	individual gas constant
S	thermal activity parameter
T_{sat}	saturation temperature

Greek symbols

α	contact angle
θ	surface orientation angle
υ	kinematic viscosity
ρ	density
σ	surface tension

Subscripts

asy	asymptotic
exp	experimental
f	liquid
g	vapor
h	high
l	low
max	maximum
pred	predicted
w	surface

fan-cooled heat sinks and single-phase liquid cooling schemes faltering in their ability to maintain acceptable device temperatures, interest has shifted to two-phase cooling schemes, which capitalize on the coolant's both latent and sensible heat rather than sensible heat alone. For over three decades, efforts at the Purdue University Boiling and Two-Phase Flow Laboratory (PU-BTPFL) have focused on research and development of two-phase cooling schemes [1,2], including two main categories of thermal solutions: (i) passive (pump-free) schemes, consisting of capillary-driven devices (heat pipes, capillary pumped loops, and loop heat pipes) [3] and pool boiling thermosyphons [4], and (ii) flow-boiling schemes, including falling film [5], channel flow boiling [6–8], mini/micro-channel flow boiling [9–11], jet-impingement [12–14], and spray [15–17], as well as hybrid cooling schemes combining the merits of mini/micro-channel flow and jet impingement [18]. Key to successful implementation of any of these schemes is the ability to predict boiling performance, especially critical heat flux (CHF). The present study is focused entirely on CHF prediction for pool boiling, which is the simplest, most prevalent, and most reliable of the different cooling schemes.

Accurate prediction of pool boiling CHF is crucial to the safety and reliability of applications spanning many industries. Since the 1940s, many efforts have been pursued to both understand CHF mechanisms and develop theoretical and empirical predictive tools. As discussed in Part I of this study [19], five main categories of theoretical models have been proposed: *bubble interference model* [20], *hydrodynamic instability model* [21–23], *macrolayer dryout model* [24], *hot/dry spot model* [25,26], and *interfacial lift-off model* [27]. Meanwhile, there have also been efforts to modify these models either theoretically or empirically in pursuit of higher predictive accuracy by accounting for effects not addressed in the original models. Overall, most modifications are based on the hydrodynamic instability model [21–23] and an early formulation based on dimensional analysis [28], which have both achieved great success in predicting pool boiling CHF. Unfortunately, most predictive tools have been validated only for a few working fluids and relatively narrow ranges of operating conditions, which inevitably limits their overall applicability. Addressing these limitations and pursuit of a more universal predictive methodology are two primary motivations for the present study.

This paper is the second part of a two-part study addressing pool boiling CHF. Part I [19] provided a detailed review of CHF models and correlations, as well as CHF trigger mechanisms. This second part will assess 18 popular CHF models and correlations using a consolidated database that the authors have amassed from 37 sources, which consists of 800 data points for 14 different fluids, and includes variations in pressure, orientation, and contact angle. Using this consolidated database, some of the models and correlations are assessed beyond their original validity ranges. Based on the assessment, the most accurate predictive methods are identified and recommended.

2. Previous CHF predicting methods

As discussed in Part I [19], pressure, surface orientation, and contact angle can have significant influences on CHF. The pressure effects are reflected in thermal properties, especially vapor density and latent heat of vaporization, which are accounted for in most models and correlations. However, surface orientation and contact angle are not accounted for in most original predictive tools, meaning these tools must be modified to address these effects. A key limitation of most predictive tools is that they were developed exclusively for the horizontal, upward-facing surface orientation ($\theta = 0°$). While different methods have been proposed to account for other surface orientations, most are purely empirical and based on data obtained only at atmospheric pressure. In addition, most pool boiling CHF papers fail to address or even mention contact angle effects.

The 18 CHF models and correlations assessed in the present paper are divided into three groups. The first group is specific to the upward-facing surface orientation and includes, aside from the original dimensionless analysis formulation of Kutateladze [28], (1) *hydrodynamic instability models* of Zuber et al. [21–23], Lienhard and Dhir [29,30], and Wang et al. [31] (which also accounts for effects of reduced pressure), (2) *bubble interference model* of Rohsenow and Griffith [20], (3) *macrolayer dryout model* of Haramura and Katto [24], (4) *hot/dry spot model* of Yagov [25], and (5) *interfacial lift-off model* of Mudawar et al. [27] and Guan et al. [32]. The second group consists of correlations incorporating the effects of orientation angle alone at atmospheric pressure, and includes studies by El-Genk and Bostanci [33], Vishnev [34], Arik and Bar-Cohen [35], Brusstar and Merte [36,37], and Chang and You [38]. The third group consists of correlations incorporating the effects of both orientation angle and contact angle at atmospheric pressure, and includes works by Kirichenko and Chernyakov [39], Theofanous and Dinh [26], Kandlikar [40], and Liao

Table 1
Predictive models and correlations for pool boiling CHF.

Author(s)	Relation(s)	Remarks
Group 1: Horizontal, upward-facing surface orientation		
Zuber et al. [21–23]	$q''_{CHF} = 0.131\rho_g h_{fg}\left[\sigma g(\rho_f - \rho_g)/\rho_g^2\right]^{1/4}$	Original hydrodynamic instability model for infinite surface
Kutateladze [28]	$q''_{CHF} = 0.16\rho_g h_{fg}\left[\sigma g(\rho_f - \rho_g)/\rho_g^2\right]^{1/4}$	Dimensional analysis
Lienhard & Dhir [29,30]	$q''_{CHF} = 0.149\rho_g h_{fg}\left[\sigma g(\rho_f - \rho_g)/\rho_g^2\right]^{1/4}$	Modified hydrodynamic instability model for finite surface
Wang et al. [31]	$q''_{CHF} = \left[0.18 - 0.14(P/P_c)^{5.68}\right]\rho_g h_{fg}\left[\sigma g(\rho_f - \rho_g)/\rho_g^2\right]^{1/4}$	Accounts for reduced pressure empirically based on liquid hydrogen data
Rohsenow & Griffith [20]	$q''_{CHF} = 0.012\rho_g h_{fg}\left(\frac{\rho_f - \rho_g}{\rho_g}\right)^{0.6}$	Bubble interference model
Haramura & Katto [24]	$q''_{CHF} = 0.721\left(\frac{A_g}{A_w}\right)^{5/8}\left(1 - \frac{A_g}{A_w}\right)^{5/16}\left[\left(\frac{\rho_f}{\rho_g}+1\right)/\left(\frac{11}{16}\frac{\rho_f}{\rho_g}+1\right)^{3/5}\right]^{5/16} \times \rho_g h_{fg}\left[\sigma(\rho_f - \rho_g)g/\rho_g^2\right]^{1/4}$ where $\frac{A_g}{A_w} = 0.0584\left(\frac{\rho_g}{\rho_f}\right)^{1/5}$	Macrolayer dryout model
Yagov [25]	$q''_{CHF,l} = 0.5\frac{h_{fg}^{81/55}\sigma^{9/11}\rho_g^{13/110}k_f^{7/110}g^{21/55}f(Pr_f)}{v_f^{1/2}c_{p,f}^{3/10}R_i^{79/110}T_{sat}^{21/22}}$ for $P/P_c < 0.001$ where $f(Pr_f) = \left(\frac{Pr_f^{9/8}}{1+2Pr_f^{1/4}+0.6Pr_f^{19/24}}\right)^{4/11}$ $q''_{CHF,h} = 0.06h_{fg}\rho_g^{3/5}\sigma^{2/5}[g(\rho_f - \rho_g)/\mu_f]^{1/5}$ for $P/P_c < 0.003$ $q''_{CHF} = (q''^3_{CHF,h} + q''^3_{CHF,l})^{1/3}$ for $0.001 < P/P_c < 0.003$	Hot/dry spot model
Guan et al. [32]	$q''_{CHF} = 0.2445\left(1 + \frac{\rho_g}{\rho_f}\right)^{1/4}\left(\frac{\rho_g}{\rho_f}\right)^{1/10}\rho_g h_{fg}\left[\sigma(\rho_f - \rho_g)g/\rho_g^2\right]^{1/4}$	Interfacial lift-off model for upward-facing surface orientation based on Mudawar et al. [27]
Mudawar et al. [27]	$q''_{CHF} = 0.151\rho_g h_{fg}\left[\sigma g(\rho_f - \rho_g)/\rho_g^2\right]^{1/4}$	Original interfacial lift-off model for pool boiling
Group 2: Predictive relations accounting for orientation effects alone at atmospheric pressure		
El-Genk & Bostanci [33]	$q''_{CHF} = [(0.229 - 4.27\times10^{-4}\theta)^{-6} + (0.577 - 2.98\times10^{-3}\theta)^{-6}]^{-1/6} \times \rho_g h_{fg}\left[\sigma g(\rho_f - \rho_g)/\rho_g^2\right]^{1/4}$	Correlated using data for HFE-7100
Vishnev [34]	$q''_{CHF} = 0.0125(190 - \theta)^{1/2}\rho_g h_{fg}\left[\sigma g(\rho_f - \rho_g)/\rho_g^2\right]^{1/4}$	Earliest and most popular correlation of orientation effects
Arik & Bar-Cohen [35]	$q''_{CHF} = 0.131(1 - 0.001117\theta + 7.79401\times10^{-6}\theta^2 - 1.37678\times10^{-7}\theta^3) \times \rho_g h_{fg}\left[\sigma g(\rho_f - \rho_g)/\rho_g^2\right]^{1/4}$	Based on hydrodynamic instability model of Zuber et al. [21–23]
Brusstar & Merte [36,37]	$q''_{CHF} = \frac{\pi}{24}\lvert\sin\theta\rvert^{1/2}\rho_g h_{fg}[\sigma g(\rho_f - \rho_g)/\rho_g^2]^{1/4}$	Derived for $90 \le \theta \le 180°$
Chang & You [38]	$q''_{CHF}/q''_{CHF,\max} = 1 - 0.0012\theta\tan(0.414\theta) - 0.122\sin(0.318\theta)$	Requires knowing CHF for upward-facing orientation
Group 3: Predictive relations accounting for orientation angle and contact angle at atmospheric pressure		
Kirichenko & Chernyakov [39]	$q''_{CHF} = 0.171\frac{(1+0.324\times10^{-3}\alpha^2)^{1/4}}{(0.018\alpha)^{1/2}}\rho_g h_{fg}\left[\sigma g(\rho_f - \rho_g)/\rho_g^2\right]^{1/4}$	First correlation to account for contact angle effects
Theofanous & Dinh [26]	$q''_{CHF} = k^{-1/2}\rho_g h_{fg}\left[\sigma g(\rho_f - \rho_g)/\rho_g^2\right]^{1/4}$ where $k = \left(1 - \frac{\sin\alpha}{2} - \frac{\pi/2-\alpha}{2\cos\alpha}\right)^{-1/2}$ [42]	Hot/dry spot model with liquid meniscus analysis, $0 \le \alpha < 90°$
Kandlikar [40]	$q''_{CHF} = \frac{1+\cos\alpha}{16}\left[\frac{2}{\pi} + \frac{\pi}{4}(1+\cos\alpha)\cos\theta\right]^{1/2} \times \rho_g h_{fg}\left[\sigma g(\rho_f - \rho_g)/\rho_g^2\right]^{1/4}$	Theoretical model based on hydrodynamic instability, $0 \le \theta \le 90°$
Liao et al. [41]	$q''_{CHF} = 0.131\left[-0.73 + \frac{1.73}{1+10^{-0.021\times(185.4-\theta)}}\right]\left[1 + \frac{55-\alpha}{100}(0.56 - 0.0013\theta)\right] \times \rho_g h_{fg}\left[\sigma g(\rho_f - \rho_g)/\rho_g^2\right]^{1/4}$	Empirical correlation, $0 \le \alpha \le 55°$ and $0 \le \theta \le 180°$

et al. [41]. Table 1 provides a summary of the 18 models and correlations segregated into the three groups.

3. New consolidated CHF database

In the present study, a total of 800 data points of saturated pool boiling CHF for flat surfaces are amassed from 37 sources [27,32,33,38,41,43–74]. The database consists of 220 data points for the upward-facing orientation from 13 sources, and 580 data points for other orientations from 24 sources. The data are obtained either directly from the original sources or extracted from digitalized figures using commercial software.

Table 2 provides key information on the individual databases incorporated in the consolidated database. Notice that some of the data are purposely excluded from the individual databases. These include enhanced CHF data such as those of Guan et al. [44], O'Hanley et al. [53], Chang and You [38], Reed and Mudawar [63], and Zhong et al. [70]. Also excluded are subcooled boiling data points such as those of Sakashita et al. [59], and data points displaying strong departure from the majority of comparable data, such as the ethanol data of Labuntsov et al. [47], and data points from Maracy and Winterton [75] and Yang et al. [76].

Part I of this study [19] showed that wall thickness can have a significant influence on pool boiling CHF. Specifically, studies have shown that thin walls artificially interfere with the CHF mechanisms and produce CHF values that are smaller than those of thick walls. Moreover, CHF for very thin walls increases with increasing wall thickness but achieves asymptotic value above a threshold thickness value. It is therefore of paramount importance to exclude very thin wall data from the consolidated database. Following is a discussion of how such data are systematically excluded.

Watwe and Bar-Cohen [77] found that CHF is related to wall thickness according to the following relation,

$$\frac{q''_{CHF}}{q''_{CHF,asy}} = \frac{S}{S+0.1}, \quad (1)$$

Table 2
CHF data for flat surfaces included in the consolidated database.

Author(s)	Pressure [MPa]	Test fluid(s)	Surface roughness [μm]	Contact angle [°]	Heater size: width × length or diameter (thickness) [mm] or area, A [mm^2]	Heater material	Inclination angle(s) [°]	Number of data points
Guan et al. [32]	0.15–0.45	Pentane, hexane, FC-72	0.15	–	25.4	Brass	0	18
Bailey et al. [43]	0.02–0.6	Pentane, methanol, water	Polished with #4000 grit emery paper	–	A = 100	Nickel-coated copper	0	22
Guan et al. [44]	0.15–0.45	Hexane,	0.15–5.5	–	25.4	Brass	0	24
Lyon et al. [45]	0.02–4.85	Liquid nitrogen, oxygen	–	–	A = 381	Platinum	0	56
Theofanous et al. [46]	Atmospheric	Water	Polished	–	20 × 40 (50)	Copper	0	3
Labuntsov et al. [47]	0.0016–0.1	Water	–	–	33	Nickel	0	4
Kim et al. [48]	Atmospheric	Water	0.041–2.36	60–70	10 × 10 (3)	Copper	0	9
Kim et al. [49]	Atmospheric	Water	0.11–2.93	7–16.3	10 × 10 (3)	Aluminum	0	9
Kwark et al. [50]	Atmospheric	Water	–	13–90	10 × 10 (3)	Al_2O_3-water/ethanol coated copper	0	37
Ahn et al. [51]	Atmospheric	Water	0.05–0.32	0–49.3	20 × 25 (0.7)	Zircaloy-4	0	10
Saeidi & Alemrajabi [52]	Atmospheric	Water	0.006–0.014	16–81	20 (10)	Aluminum alloy 2011	0	22
O'Hanley et al. [53]	Atmospheric	Water	0.01–2.69	5–113	10 × 20 (0.25)	Indium tin oxide-sapphire	0	5
Park et al. [54]	Atmospheric	Water	Polished	56.7	20 × 25 (0.5)	Silicon wafer	0	1
Guo & El-Genk [55]	Near atmospheric	Water	Polished with #1200 silicon carbide sand paper	–	50.8 (12.8)	Copper	90–180	14
Beduz et al. [56]	Atmospheric	Liquid nitrogen	–	–	50 × 50 (6)	Copper, aluminum	0–176	14
Nishio & Chandratilleke [57]	Atmospheric	Liquid helium	0.027–4.35	–	20 (30)	Copper	0–179	5
El-Genk & Bostanci [33]	Near atmospheric	HFE-7100	Polished with #1500 emery paper	–	10 × 10 (1.63)	Copper	0–180	8
Katto et al. [58]	0.025–0.1	Water	–	–	10	Copper	0–90	20
Sakashita et al. [59]	Atmospheric	Water	–	–	5 × 48	Copper	90–170	12
Sakashita [60]	0.1–3	Ethanol, R-141b, water	Polished with #2000 emery paper	–	7	Copper	90	32
Mudawar et al. [27]	Atmospheric	Water, FC-72	Blasted with 10 μm particles	–	12.7 × 12.7 (2.5), 12 × 62 (2.5)	Copper	90	15
Monde et al. [61]	Atmospheric	Water, ethanol	–	–	10 × 20–10 × 50	Copper	90	12
Howard & Mudawar [62]	Atmospheric	FC-72	Polished with Crocus cloth	–	12.7 × 12.7, 3.2 × 35	Copper	90–180	26
Chang & You [38]	Atmospheric	FC-72	Polished with Brasso	–	10 × 10 (1.5)	Copper	0–180	6
Reed & Mudawar [63]	Atmospheric	FC-72, FC-87	Polished with 0.05 μm grit paper	–	12.7 (16)	Copper	0–180	10
Jergel & Stevenson [64]	Atmospheric	Liquid helium	Polished	–	15 (10)	Copper	0–180	3
Bewilogua et al. [65]	0.006–3	Liquid helium, nitrogen, hydrogen	Ground with F9 emery cloth	–	A = 290, 490	Copper	0–165	153
Deev et al. [66]	0.1–0.225	Liquid helium	Polished	–	30 × 30	Copper	0–90	38
Gogonin & Kutateladze [67]	0.1–5.2	Ethanol	–	–	5 × 150–50 × 150 (0.5)	Stainless steel	0–180	136
Liaw & Dhir [68]	Atmospheric	R-113, water	polished with #00 emery paper	0–107	6.3 × 10.3	Copper	90	6
Priarone [69]	Atmospheric	FC-72, HFE-7100	0.6	–	A = 707	Copper	0–175	10
Liao et al. [41]	Atmospheric	Water	0.105–0.197	0–55	20	TiO_2 coated copper	0–180	15
Zhong et al. [70]	Atmospheric	Water	–	–	100 × 100	Copper	90–175	5
Kim et al. [71]	Atmospheric	Water	–	–	15 × 35	Copper	90–180	12
Kwark et al. [72]	0.02–0.2	Water	–	–	7.5 × 7.5 (3), 10 × 10 (3), 15 × 15 (3), 20 × 20 (3)	Copper	0–180	13
Rainey & You [73]	Atmospheric	FC-72	Polished with Brasso	–	20 × 20 (3.2), 50 × 50 (3.2)	Copper	0–180	12
Wang & Dhir [74]	Atmospheric	Water	<0.02	18–90	63 × 103	Copper	90	3

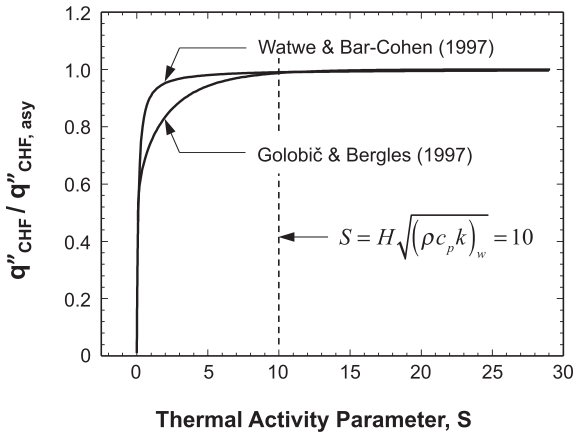

Fig. 1. Variations of CHF with thermal activity parameter.

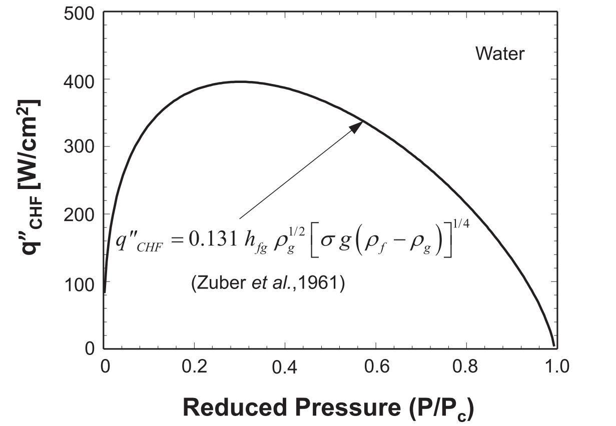

Fig. 2. Variation of pool boiling CHF for water with reduced pressure based on hydrodynamic instability model of Zuber et al. [21–23].

where $q''_{CHF,\ asy}$ is the asymptotic CHF, S the 'thermal activity' parameter, defined as

$$S = H\sqrt{(\rho c_p k)_w}, \quad (2)$$

and H the wall thickness. This relationship yields 90% of asymptotic CHF at $S = 1$ and 99% at $S = 10$. Golobič and Bergles [78] recommended an alternative correlation to account for wall thickness effects,

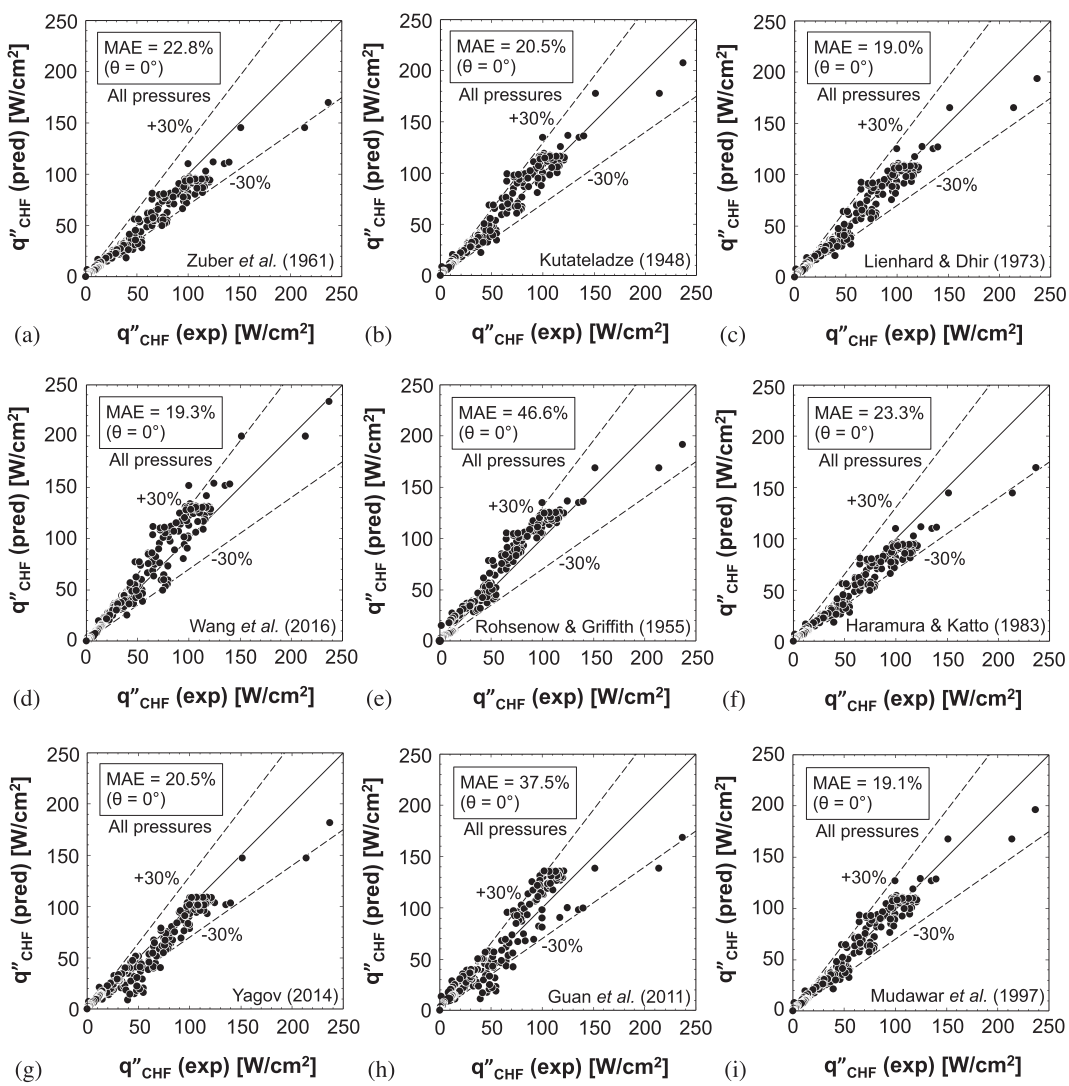

Fig. 3. Comparison of data from consolidated database for horizontal, upward-facing orientation and different pressures with predictions of different models and correlations: (a) Zuber [21–23], (b) Kutateladze [28], (c) Lienhard and Dhir [29,30], (d) Wang et al. [31], (e) Rohsenow and Griffith [20], (f) Haramura and Katto [24], (g) Yagov [25], (h) Guan et al. [32], and (i) Mudawar et al. [27].

$$\frac{q''_{CHF}}{q''_{CHF,asy}} = 1 - \exp\left[-\left(\frac{S}{2.44}\right)^{0.8498} - \left(\frac{S}{2.44}\right)^{0.0581}\right]. \quad (3)$$

Fig. 1 shows variations of CHF with thermal activity parameter using Eqs. (1) and (3). Despite differences between predictions based on the two expressions for $S < 10$, both show negligible influence for $S \geq 10$. Therefore, this value of $S = 10$ was used to guide the exclusion of thin wall data. This value yields minimum wall thickness values for common wall materials such as copper, aluminum, and stainless steel of 0.27, 0.41, and 0.57 mm, respectively. To ensure that the consolidated database is independent of the artificial wall thickness effect, all data points for wall thicknesses below 0.25 mm, such as those of Sakashita and Ono [79] and Kim et al. [42], have been excluded.

Overall, the consolidated database consists of 800 pool boiling CHF data points from 37 sources with the following coverage:

- Working fluids: water, pentane, hexane, methanol, ethanol, R-141b, R-113, FC-72, FC-87, HFE-7100, liquid nitrogen, oxygen, helium, and hydrogen.
- Pressure: $0.0016 \leq P \leq 5.2$ MPa.
- Orientation angle: $0 \leq \theta \leq 180°$.
- Contact angle: $0 < \alpha \leq 113°$.

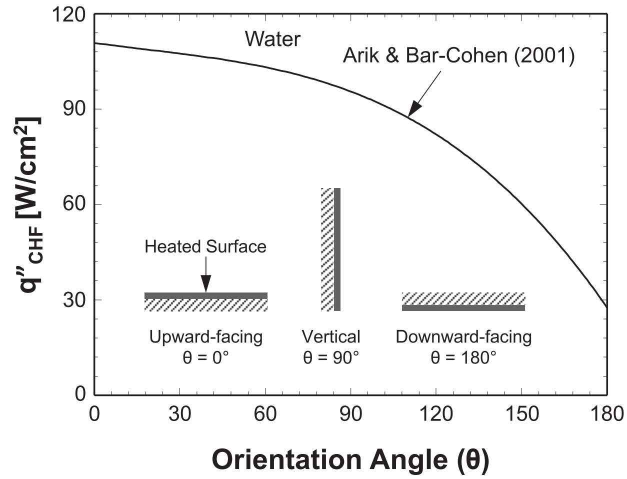

Fig. 5. Variation of pool boiling CHF for water with surface orientation angle.

4. Assessment of previous models and correlations

4.1. Horizontal, upward-facing orientation

Despite fundamental differences among the 9 models and correlations for the horizontal, upward-facing orientation (group 1

Table 3
Mean absolute errors of nine models and correlations in predicting individual CHF databases for the horizontal, upward-facing orientation.

Database source	Fluid(s)	Mean absolute error [%]								
		Zuber [21–23]	Kutateladze [28]	Lienhard & Dhir [29,30]	Wang et al. [31]	Rohsenow & Griffith [20]	Haramura & Katto [24]	Yagov [25]	Guan et al. [32]	Mudawar et al. [27]
Guan et al. [32]	Pentane, hexane, FC-72	17.7	9.3	9.9	14.0	14.5	18.3	14.6	6.6	9.5
Bailey et al. [43]	Pentane, methanol, water	22.3	14.1	16.1	16.9	19.6	22.6	26.7	20.4	15.6
Guan et al. [44]	Hexane	14.7	6.1	6.2	17.1	6.3	15.3	8.4	7.5	5.8
Lyon et al. [45]	Liquid nitrogen, oxygen	21.8	23.5	18.5	26.4	57.3	22.4	22.6	42.3	19.2
Labuntsov et al. [47]	Water	36.9	26.0	28.2	23.1	13.2	37.0	61.2	56.5	27.4
Katto et al. [58]	Water	18.6	18.2	16.5	24.6	20.6	18.7	37.1	34.6	16.8
Bewilogua et al. [65]	Liquid helium, nitrogen, hydrogen	31.7	29.9	29.5	13.6	70.4	32.1	26.3	59.2	29.4
Deev et al. [66]	Liquid helium	41.8	45.0	43.8	16.8	163.7	42.6	31.1	88.3	44.0
Gogonin & Kutateladze [67]	Ethanol	14.1	10.6	8.7	20.7	17.5	14.6	8.7	19.9	8.8
Kwark et al. [72]	Water	7.2	28.6	19.7	44.6	34.0	7.1	9.4	9.8	21.3
All data		22.8	20.5	19.0	19.3	46.6	23.3	20.5	37.5	19.1

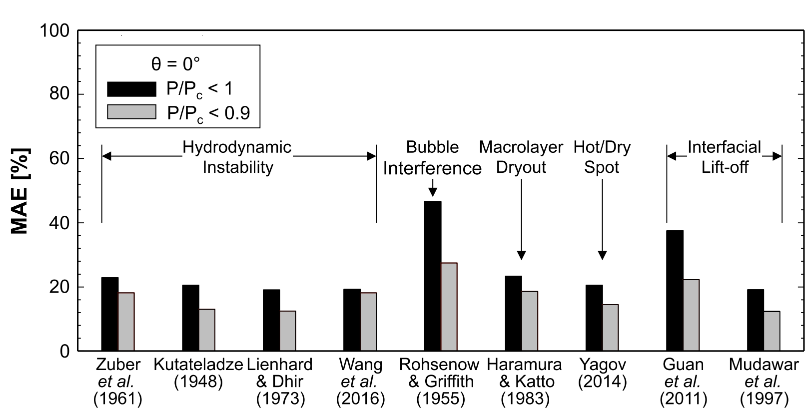

Fig. 4. Mean absolute errors of nine models and correlations in predicting data for horizontal, upward-facing orientation, segregated relative to two ranges of reduced pressure.

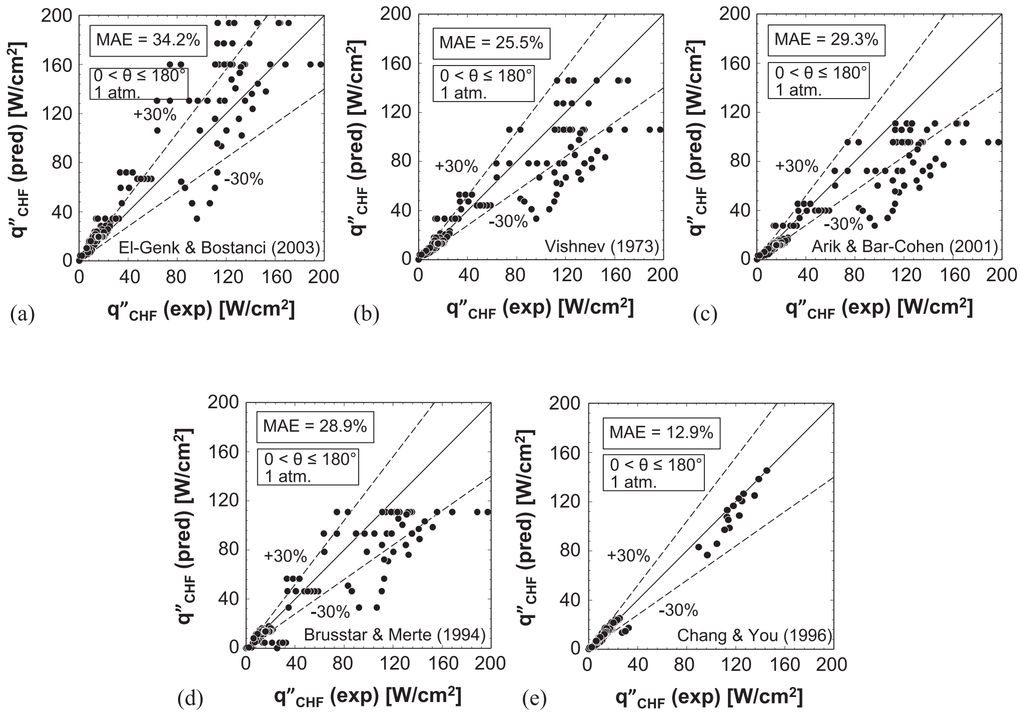

Fig. 6. Comparison of atmospheric pressure CHF data for different orientations (excluding $\theta = 0°$) with predictions of empirical correlations: (a) El-Genk and Bostanci [33], (b) Vishnev [34], (c) Arik and Bar-Cohen [35], (d) Brusstar and Merte [36,37], and (e) Chang and You [38].

Table 4
Mean absolute errors of seven correlations in predicting individual atmospheric pressure CHF databases for different surface orientations excluding θ=0°.

Database source	Fluid(s)	Mean absolute error [%]						
		El-Genk & Bostanci [33]	Vishnev [34]	Arik & Bar-Cohen [35]	Brusstar & Merte [36,37]	Chang & You [38]	Eq. (5a)	Eq. (5b)
Theofanous et al. [46]	Water	16.7	12.2	33.2	–	–	24.0	23.0
Park et al. [54]	Water	52.8	15.0	12.5	–	–	0.5	0.8
Guo & El-Genk [55]	Water	86.3	43.4	25.2	42.7	–	22.9	24.0
Beduz et al. [56]	Liquid nitrogen	42.6	10.8	14.6	16.8	15.5	15.5	15.7
Nishio & Chandratilleke [57]	Liquid helium	34.8	17.2	22.3	7.8	29.3	13.0	12.4
El-Genk & Bostanci [33]	Hfe-7100	11.0	22.0	30.9	33.0	5.0	28.7	27.7
Sakashita et al. [59]	Water	14.1	43.4	49.3	37.2	–	41.6	40.8
Mudawar et al. [27]	Water, FC-72	19.3	21.4	29.0	17.6	–	19.5	18.4
Monde et al. [61]	Water, ethanol	29.0	14.7	22.9	10.6	–	12.6	11.4
Howard & Mudawar [62]	FC-72	17.4	20.0	32.4	32.6	12.5	25.3	24.3
Chang & You [38]	FC-72	58.9	34.2	34.5	18.4	6.3	8.5	7.7
Reed & Mudawar [63]	FC-72, FC-87	18.4	16.3	26.5	38.4	14.1	26.2	25.3
Jergel & Stevenson [64]	Liquid helium	17.3	24.5	25.5	50.5	13.9	34.2	33.3
Priarone [69]	FC-72, HFE-7100	17.8	17.0	29.7	19.7	9.0	23.1	22.0
Liao et al. [41]	Water	33.0	14.8	17.8	35.3	16.0	19.2	18.6
Zhong et al. [70]	Water	16.1	43.1	48.9	37.8	–	42.3	41.5
Kim et al. [71]	Water	26.3	40.0	46.2	36.8	–	40.2	39.4
Kwark et al. [72]	Water	41.6	11.7	12.8	30.6	13.6	12.8	12.7
Rainey & You [73]	FC-72	92.6	46.5	28.0	32.6	10.6	22.0	23.5
Total		34.2	25.5	29.3	28.9	12.9	23.8	23.3

in Table 1), they all predict fairly similar CHF trends relative to reduced pressure. Using the Zuber model [21–23] as example, Fig. 2 shows that CHF first increases to maximum value with increasing pressure, before decreasing to near zero value at the critical pressure. This section will assess the predictive accuracy of the 9 models and correlations intended for the horizontal, upward-facing orientation.

When comparing the consolidated database to predictions of the previous models or correlations, the thermophysical properties for different working fluids are obtained using NIST's REFPROP 8.0 software [80], excepting those for FC-72, which are obtained from 3 M Company. The parameter used to assess the accuracy of individual models or correlations is mean absolute error (MAE), which is defined as

$$\mathrm{MAE} = \frac{1}{N}\sum \frac{\left|q''_{CHF,pred} - q''_{CHF,exp}\right|}{q''_{CHF,exp}} \times 100\%, \quad (4)$$

where $q''_{CHF,\,pred}$ and $q''_{CHF,\,exp}$ are the predicted and measured CHF, respectively.

Shown in Figs. 3(a)–(i) are comparisons of horizontal, upward-facing surface data at different reduced pressures with predictions of the 9 models and correlations. Overall, the hydrodynamic instability model of Zuber [21–23], Fig. 3(a), macrolayer dryout model of Haramura and Katto [24], Fig. 3(f), and hot/dry spot model of Yagov [25], Fig. 3(g), underestimate the consolidated CHF database, while the Kutateladze relation [28], Fig. 3(b), and bubble interference model of Rohsenow and Griffith [20], Fig. 3(e), overestimate. In contrast, predictions of the modified hydrodynamic instability models of Lienhard and Dhir [29,30], Fig. 3(c), and Wang et al. [31], Fig. 3(d), and the interfacial lift-off models of Guan et al. [32], Fig. 3(h), and Mudawar et al. [27], Fig. 3(i), show closer agreement. Table 3 provides detailed MAEs of the 9 models and correlations against data from individual sources. Notice that, despite its seemingly close distribution, the Guan et al. model shows a comparatively large MAE of 37.5%. Overall, the most accurate predictions are achieved with the models of Lienhard and Dhir and Mudawar et al., with virtually identical MAEs of 19.0% and 19.1%, respectively. Notice that the Wang et al. model also shows a low MAE of 19.3% but a wider spread, as shown in Fig. 3(d).

Therefore, the models of Lienhard and Dhir and Mudawar et al. are recommended for CHF prediction for the horizontal, upward-facing orientation. Notice that the interfacial lift-off model of Mudawar et al. [27] was originally devised for the vertical orientation, but does possess the ability to predict CHF for other orientations using a separated flow sub-model. However, the simple form of this model for the vertical orientation, Table 1, was found in a follow-up study by Howard and Mudawar [62] to predict CHF of the horizontal, upward-facing orientation as well, given the very weak orientation effect on CHF for $0 < \theta < 90°$.

Fig. 4 compares MAEs of the nine models and correlations for $P/P_c < 1$ and $P/P_c < 0.9$. Segregating pressure data in this manner is intended to highlight the relatively large uncertainty in CHF prediction close to the critical pressure. Notice how, by focusing on data in the range of $P/P_c < 0.9$ rather than the entire pressure range, MAEs for all nine models and correlations are reduced further, from 22.8 to 18.2%, 20.5 to 13.0%, 19.0 to 12.5%, 19.3 to 18.1%, 46.6 to 27.5%, 23.3 to 18.6%, 20.5 to 14.5%, 37.5 to 22.3%, and 19.1 to 12.4%, for Zuber et al., Kutateladze, Lienhard and Dhir, Wang et al., Rohsenow and Griffith, Haramura and Katto, Yagov, Guan et al., and Mudawar et al., respectively. Improvements for the models of Rohsenow and Griffith and Guan et al. are especially noteworthy. Overall, considering data only in the range of $P/P_c < 0.9$, best predictions are achieved with the models of Mudawar et al. and Lienhard and Dhir, evidenced by their smallest MAEs of 12.4% and 12.5%, respectively.

4.2. Inclined orientations at atmospheric pressure

Using the correlation of Arik and Bar-Cohen [35] as example, Fig. 5 shows the variation of CHF with orientation angle. It shows CHF decreases slightly between $\theta = 0$ and 90°, and more appreciably between 90 and 180°. This general trend agrees with the majority of experiments involving orientations effects [33,56,69,81–83].

Shown in Figs. 6(a)–(e) are comparisons of measured atmospheric pressure CHF data for inclined surfaces (excluding $\theta = 0°$) with predictions of the five empirical correlations from group 2 in Table 1. While the correlation of Chang and You [38], Fig. 6(e), shows the lowest MAE of 12.9%, it suffers the disadvantage that it requires prior knowledge of CHF value for the horizontal upward-facing orientation ($\theta = 0°$) corresponding to maximum CHF; only 114 data points could be used to assess its accuracy. Table 4 shows detailed MAEs of the five correlations against atmospheric pressure data from individual sources. It shows fair accuracy for the Vishnev correlation [34], with a MAE of 25.5%, and higher MAEs for the correlations of El-Genk and Bostanci [33], Arik and Bar-Cohen [35], and Brusstar and Merte [36,37].

As discussed earlier, the models of Lienhard and Dhir [29,30] and Mudawar et al. [27] provide the highest accuracy in predicting CHF for the horizontal, upward-facing orientation. Replacing $q''_{CHF,\,max}$ in the correlation of Chang and You [38] with the models of Lienhard and Dhir and Mudawar et al. yields the following two new relations for orientation effects, respectively,

$$q''_{CHF} = 0.149\rho_g h_{fg}\left[\sigma g(\rho_f - \rho_g)/\rho_g^2\right]^{1/4}[1 - 0.0012\theta\tan(0.414\theta) - 0.122\sin(0.318\theta)] \tag{5a}$$

and $$q''_{CHF} = 0.151\rho_g h_{fg}\left[\sigma g(\rho_f - \rho_g)/\rho_g^2\right]^{1/4}[1 - 0.0012\theta\tan(0.414\theta) - 0.122\sin(0.318\theta)]. \tag{5b}$$

MAEs of Eqs. (5a) and (5b) against atmospheric pressure data from individual sources are provided in Table 4. Figs. 7(a) and (b) compare atmospheric pressure CHF data from the consolidated database for different orientations (excluding $\theta = 0°$) with predictions based

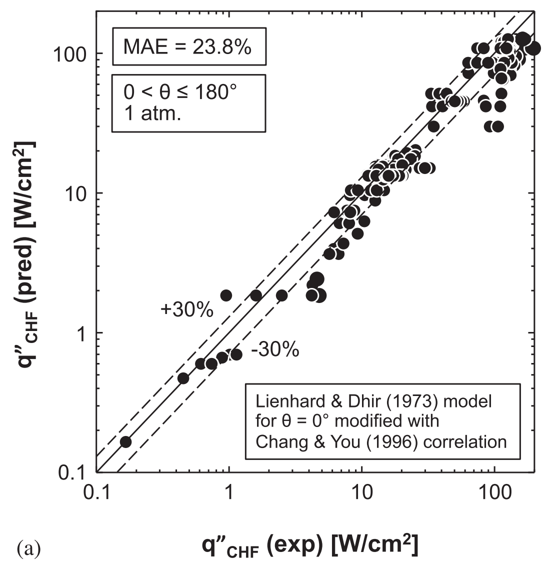

(a)

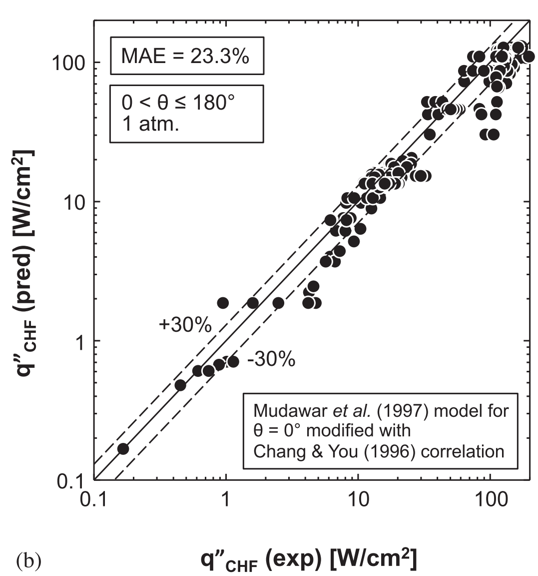

(b)

Fig. 7. Comparison of atmospheric pressure CHF data for different orientations (excluding $\theta = 0°$) with predictions of (a) Lienhard and Dhir model [29,30] modified with Chang and You correlation [38], Eq. (5a), and (b) Mudawar et al. model [27] modified with Chang and You correlation, Eq. (5b).

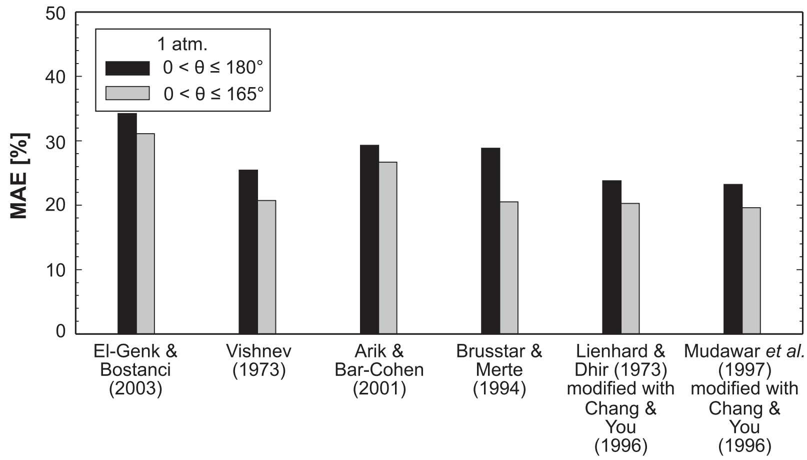

Fig. 8. Mean absolute errors of six approaches to predicting atmospheric CHF data for inclined surfaces, segregated relative to two ranges of orientation angle excluding $\theta = 0°$.

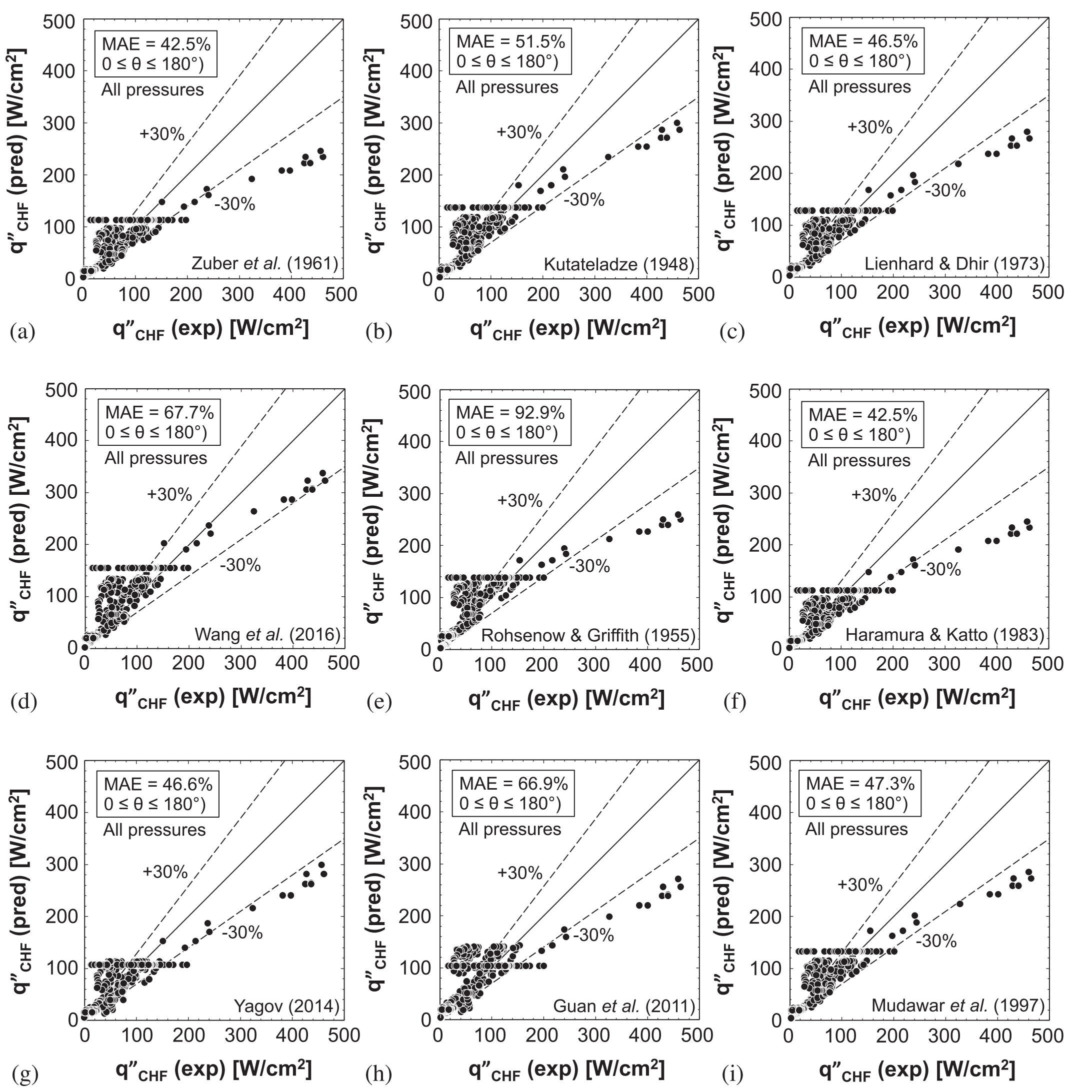

Fig. 9. Comparison of experimental data for all pressures and all orientation angles (including $\theta = 0°$) with predictions of different models and correlations: (a) Zuber [21–23], (b) Kutateladze [28], (c) Lienhard and Dhir [29,30], (d) Wang et al. [31], (e) Rohsenow and Griffith [20], (f) Haramura and Katto [24], (g) Yagov [25], (h) Guan et al. [32], and (i) Mudawar et al. [27].

on Eqs. (5a) and (5b), respectively. They show MAEs of 23.8% and 23.3%, respectively, which are lower than that of Vishnev [34].

Fig. 8 compares MAEs of the same five empirical correlations from group 2 in predicting atmospheric pressure CHF data for inclined surfaces, but with orientations segregated into the entire range of $0 < \theta \leq 180°$ and a narrower range of $0 < \theta \leq 165°$, excluding $\theta = 0°$. Notice that the Chang and You correlation is replaced by Eqs. (5a) and (5b). One reason for the angle range segregation is that, to the authors' best knowledge, none of the available CHF models or correlations can accurately predict CHF for the horizontal, downward-facing orientation ($\theta = 180°$). This is reflected in the narrower range reducing MAE from 34.2 to 31.1%, 25.5 to 20.7%, 29.3 to 26.7%, 28.9 to 20.5%, 23.8 to 20.3%, and 23.3% to 19.6% for El-Genk and Bostanci [33], Vishnev [34], Arik and Bar-Cohen [35], Brusstar and Merte [36,37], and new combined relations based the Lienhard and Dhir model [29,30] modified with the Chang and You correlation [38], Eq. (5a), and the Mudawar et al. model [27] modified with the Chang and You correlation, Eq. (5b), respectively.

4.3. Inclined orientations at different pressures

As discussed earlier, several models and correlations show good accuracy in predicting the influence of pressure on pool boiling CHF for the horizontal, upward-facing orientation. And several correlations have shown some success in predicting surface orientation effects at one atmosphere. The next step in the present assessment study is therefore to investigate effectiveness of predictive tools in capturing simultaneously the pressure and orientation effects.

Figs. 9(a)–(i) compare predictions of the nine models and correlations from group 1 in Table 1 with CHF data from the consolidated database for all pressures and all orientation angles, including $\theta = 0°$. Table 5 provides complementary assessment of the same models and correlations against individual databases, again for all pressures and all orientation angles, including $\theta = 0°$. Overall, Figs. 9(a)–(i) show large MAEs for all nine models and correlations, especially for lower CHF values, which, as shown in Table 5, correspond to liquid helium. This can be explained by the fact that these models and correlations are originally intended only for the horizontal, upward-facing orientation.

Figs. 10(a)–(f) compare predictions of the four empirical correlations from group 2 in Table 1, along with those of Eqs. (5a) and (5b), with the consolidated database for all pressures and all orientation angles, including $\theta = 0°$. Table 6 provides additional MAE details for the same predictive tools, again for all pressures and all orientation angles, including $\theta = 0°$. Being intended for different surface orientations, Figs. 10(a)–(f) show better predictive accuracies than those of group 1. Nonetheless, their MAEs are still large, with the smallest MAE of 26.9% achieved by Vishnev [34]. On the other hand, the new modified correlations provide the most superior predictions, supported by MAEs of 26.0% and 25.9% for Eqs. (5a) and (5b), respectively.

Fig. 11(a) shows the distributions of MAEs from Figs. 10(a)–(f) for specific orientation angles of 90°, 135°, 165°, and 180°. This figure shows that a significant part of predictive error is associated with data measured at $\theta = 180°$. Fig. 11(b) lends further support of poor predictions associated with orientation angles nearing 180°. It shows that orientation angles confined to $\theta \leq 165°$ (including $\theta = 0°$) reduce MAEs considerably compared to Figs. 10(a)–(f). As

Table 5
Comparison of individual CHF databases of all orientations and all pressures with predictions of previous models or correlations.

Database source	Fluid(s)	Mean absolute error [%]								
		Zuber et al. [21–23]	Kutateladze [28]	Lienhard & Dhir [29,30]	Wang et al. [31]	Rohsenow & Griffith [20]	Haramura & Katto [24]	Yagov [25]	Guan et al. [32]	Mudawar et al. [27]
Guan et al. [32]	Pentane, hexane, FC-72	17.7	9.3	9.9	14.0	14.5	18.3	14.6	6.6	9.5
Bailey et al. [43]	Pentane, methanol, water	22.3	14.1	16.1	16.9	19.5	22.6	26.7	20.4	15.6
Guan et al. [44]	Hexane	14.7	6.1	6.2	17.1	6.3	15.3	8.4	7.5	5.8
Lyon et al. [45]	Liquid nitrogen, oxygen	21.8	23.5	18.5	26.4	57.3	22.4	22.6	42.3	19.2
Labuntsov et al. [47]	Water	36.9	26.0	28.2	23.1	13.2	37.0	61.2	56.5	27.4
Theofanous et al. [46]	Water	33.2	18.4	24.0	8.2	18.3	33.5	38.3	40.4	23.0
Park et al. [54]	Water	12.5	6.8	0.5	20.2	6.9	12.9	19.2	21.9	0.8
Katto et al. [58]	Water	19.7	19.2	17.8	24.8	20.8	19.9	38.3	35.6	18.1
Bewilogua et al. [65]	Liquid helium, nitrogen, hydrogen	37.0	47.4	42.6	42.1	127.7	37.1	49.0	84.2	43.3
Deev et al. [66]	Liquid helium	43.5	58.9	53.0	30.0	200.4	44.0	49.6	117.9	54.1
Gogonin & Kutateladze [67]	Ethanol	39.1	52.6	45.5	63.9	69.8	39.0	44.4	76.4	46.7
Kwark et al. [72]	Water	7.2	28.6	19.7	44.6	34.0	7.1	9.4	9.8	21.3
Sakashita [60]	Ethanol, R-141b, water	37.2	24.8	29.5	17.3	22.5	37.6	33.5	27.7	28.6
Guo & El-Genk [55]	Water	229.0	301.8	274.2	352.0	302.3	227.7	203.8	193.6	279.2
Beduz et al. [56]	Liquid nitrogen	71.9	107.1	92.8	133.0	154.9	71.1	66.6	89.1	95.4
Nishio & Chandratilleke [57]	Liquid helium	74.6	95.3	87.4	108.7	204.8	74.2	105.2	132.3	88.8
El-Genk & Bostanci [33]	HFE-7100	66.0	75.9	71.7	86.8	107.3	65.8	61.8	71.7	72.3
Sakashita et al. [59]	Water	23.3	19.6	19.6	24.6	19.6	23.5	26.7	28.0	19.4
Mudawar et al. [27]	Water, FC-72	17.6	7.6	7.8	15.3	37.7	18.1	28.5	8.3	7.1
Monde et al. [61]	Water, ethanol	10.5	10.0	5.4	22.9	17.6	10.9	23.9	14.9	6.0
Howard & Mudawar [62]	FC-72	32.8	29.4	30.6	32.4	67.4	32.9	37.3	30.3	30.4
Chang &You [38]	FC-72	143.2	184.8	166.8	220.4	307.9	142.3	123.0	170.8	169.5
Reed & Mudawar [63]	FC-72, FC-87	70.0	82.3	76.6	96.1	122.5	69.8	67.4	77.7	77.6
Jergel & Stevenson [64]	Liquid helium	123.9	144.6	136.3	165.3	278.4	123.3	159.9	196.3	137.7
Priarone [69]	FC-72, HFE-7100	42.3	47.8	45.4	841.9	87.2	42.2	41.7	45.6	45.7
Liao et al. [41]	Water	62.8	83.2	73.4	104.7	83.4	62.7	60.8	60.4	75.2
Zhong et al. [70]	Water	23.7	24.5	24.2	31.8	24.5	23.6	23.4	23.3	24.2
Kim et al. [71]	Water	8.5	15.6	10.2	30.0	15.7	8.7	13.7	16.0	10.8
Kwark et al. [72]	Water	62.3	89.2	76.2	112.9	89.4	62.2	59.1	57.8	78.6
Rainey & You [73]	FC-72	179.9	240.7	217.3	283.3	387.9	178.2	149.2	223.2	221.5
Total		42.5	51.5	46.5	67.7	92.9	42.5	46.6	66.9	47.3

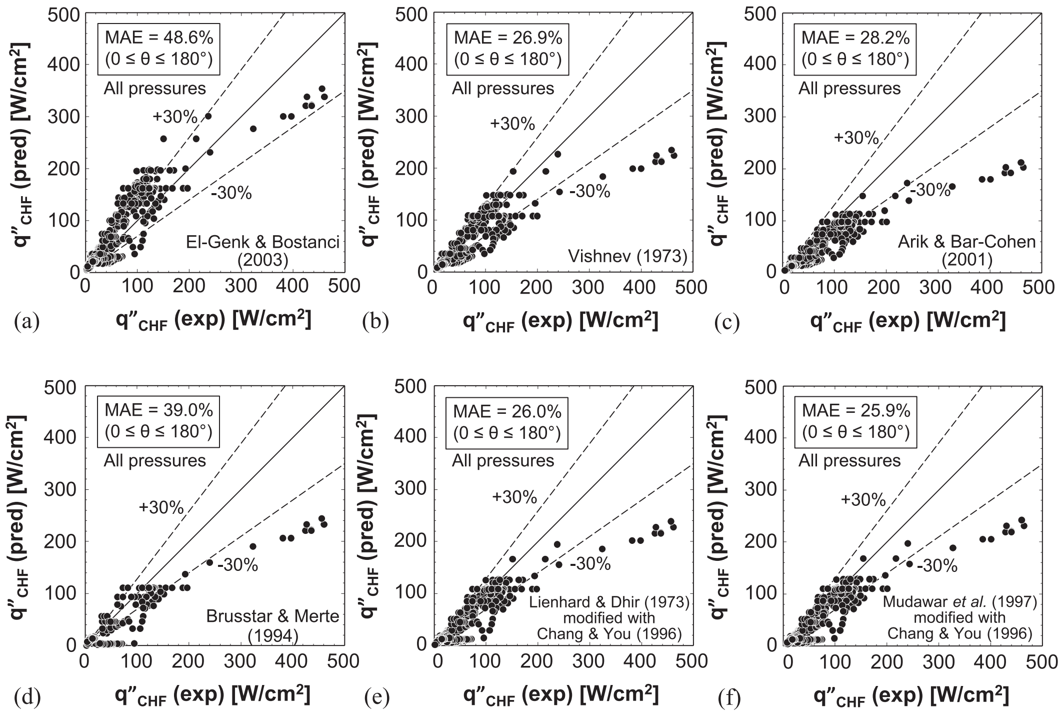

Fig. 10. Comparison of experimental data for all pressures and all orientation angles (including $\theta = 0°$) with predictions of empirical correlations: (a) El-Genk and Bostanci [33], (b) Vishnev [34], (c) Arik and Bar-Cohen [35], (d) Brusstar and Merte [36,37], (e) Lienhard and Dhir model [29,30] modified with Chang and You correlation [38], Eq. (5a), and (f) Mudawar et al. model [27] modified with Chang and You correlation, Eq. (5b).

Table 6
Comparison of individual CHF databases for all orientations and all pressures with predictions of previous empirical correlations for orientation effects, as well as those of the new modified models.

Database source	Fluid(s)	Mean absolute error [%]					
		El-Genk & Bostanci [33]	Vishnev [34]	Arik & Bar-Cohen [35]	Brusstar & Merte [36,37]	Eq. (5a)	Eq. (5b)
Guan et al. [32]	Pentane, hexane, FC-72	43.7	11.2	17.7	–	9.9	9.5
Bailey et al. [43]	Pentane, methanol, water	41.2	15.2	22.3	–	16.1	15.6
Guan et al. [44]	Hexane	48.9	12.1	14.7	–	6.2	5.8
Lyon et al. [45]	Liquid nitrogen, oxygen	75.0	31.8	21.8	–	18.5	19.2
Labuntsov et al. [47]	Water	19.6	24.2	36.9	–	28.2	27.4
Theofanous et al. [46]	Water	16.7	12.2	33.2	–	24.0	23.0
Park et al. [54]	Water	52.8	15.0	12.5	–	0.5	0.8
Katto et al. [58]	Water	46.3	22.4	20.5	26.4	18.0	18.3
Bewilogua et al. [65]	Liquid helium, nitrogen, hydrogen	54.7	25.5	27.2	17.4	23.7	23.6
Deev et al. [66]	Liquid helium	92.1	43.5	36.1	45.7	43.2	44.2
Gogonin & Kutateladze [67]	Ethanol	48.7	27.8	30.7	92.9	35.4	35.3
Kwark et al. [72]	Water	83.9	38.4	7.2	–	19.7	21.3
Sakashita [60]	Ethanol, R-141b, water	14.3	39.8	45.6	37.2	38.5	37.8
Guo & El-Genk [55]	Water	86.3	43.4	25.2	42.7	22.9	24.0
Beduz et al. [56]	Liquid nitrogen	42.6	10.8	14.6	16.8	15.5	15.7
Nishio & Chandratilleke [57]	Liquid helium	34.8	17.2	22.3	7.8	13.0	12.4
El-Genk & Bostanci [33]	HFE-7100	11.0	22.0	30.9	33.0	28.6	27.7
Sakashita et al. [59]	Water	14.0	43.4	49.3	37.1	41.6	40.8
Mudawar et al. [27]	Water, FC-72	19.3	21.4	29.0	17.6	19.5	18.4
Monde et al. [61]	Water, ethanol	29.0	14.6	22.9	10.5	12.6	11.4
Howard & Mudawar [62]	FC-72	17.4	20.0	32.4	32.6	25.3	24.3
Chang & You [38]	FC-72	58.9	34.2	34.5	18.4	8.5	7.7
Reed & Mudawar [63]	FC-72, FC-87	18.3	16.3	26.5	38.4	26.2	25.3
Jergel & Stevenson [64]	Liquid helium	17.3	24.5	25.5	50.5	34.2	33.3
Priarone [69]	FC-72, HFE-7100	17.8	17.0	29.7	19.7	23.1	22.0
Liao et al. [41]	Water	33.0	14.8	17.8	35.2	19.2	18.6
Zhong et al. [70]	Water	16.1	43.1	48.9	37.8	42.3	41.5
Kim et al. [71]	Water	26.3	40.0	46.2	36.8	40.2	39.4
Kwark et al. [72]	Water	41.6	11.7	12.8	30.6	12.8	12.7
Rainey & You [73]	FC-72	92.6	46.5	28.0	32.6	22.0	23.5
Total		48.6	26.9	28.2	39.0	26.0	25.9

shown in Fig. 11(b), MAEs of the three correlations are reduced from 26.9 to 24.1%, 28.2 to 25.1%, and 39.0 to 23.8%, based on Vishnev [34], Arik and Bar-Cohen [35], and Brusstar and Merte [36,37], while MAE of the correlation based on El-Genk & Bostanci [33] hardly changes. In terms of the modified models, Fig. 11(b) shows that confining orientation angle to $\theta \leq 165°$ reduces the MAEs for Eqs. (5a) and (5b), from 26.0 to 20.7% and 25.9 to 20.7%, respectively. Here too, Eqs. (5a) and (5b) provide the most accurate predictions.

4.4. Contact angle effects

The effects of contact angle on pool boiling CHF have been investigated both experimentally and theoretically. Fig. 12 shows an example of these effects, predicted according to Kandlikar's model [40], which shows CHF decreasing monotonically with increasing contact angle. To the authors' best knowledge, only four models and correlations addressing contact angle effects can be found in the literature. They consist of an early correlation by Kirichenko and Chernyakov [39], a model by Theofanous and Dinh [26], a model by Kandlikar [40], and an empirical correlation by Liao et al. [41], which are identified as group 3 in Table 1. It should be noted that both Kandlikar's model and the correlation of Liao et al. also account for surface orientation effects. Also, the k value in Theofanous and Dinh's model is calculated using a model by Kim et al. [42].

Fig. 13 compares predictions of the four models and correlations from group 3 with CHF data from the consolidated database for $0 \leq \alpha \leq 90°$. It shows that the predictions of the Kirichenko and Chernyakov's correlation and Theofanous and Dinh's model deviate greatly from the data. Kandlikar's model and the correlation of Liao et al. provide better accuracies, with MAEs of 22.6% and 23.4%, respectively. Table 7 provides detailed MAEs of the four predictive methods against individual databases.

It is worth noting that the four predictive tools are limited to hydrophilic liquids ($0 \leq \alpha \leq 90°$). This points to a need for models or correlations that would account for a broader range of contact angles, including hydrophobic liquids ($90° \leq \alpha \leq 180°$).

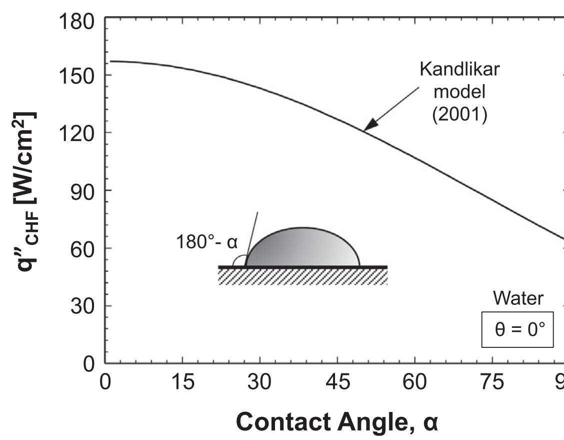

Fig. 12. Effects of contact angle on pool boiling CHF for water from a horizontal upward-facing surface at one atmosphere.

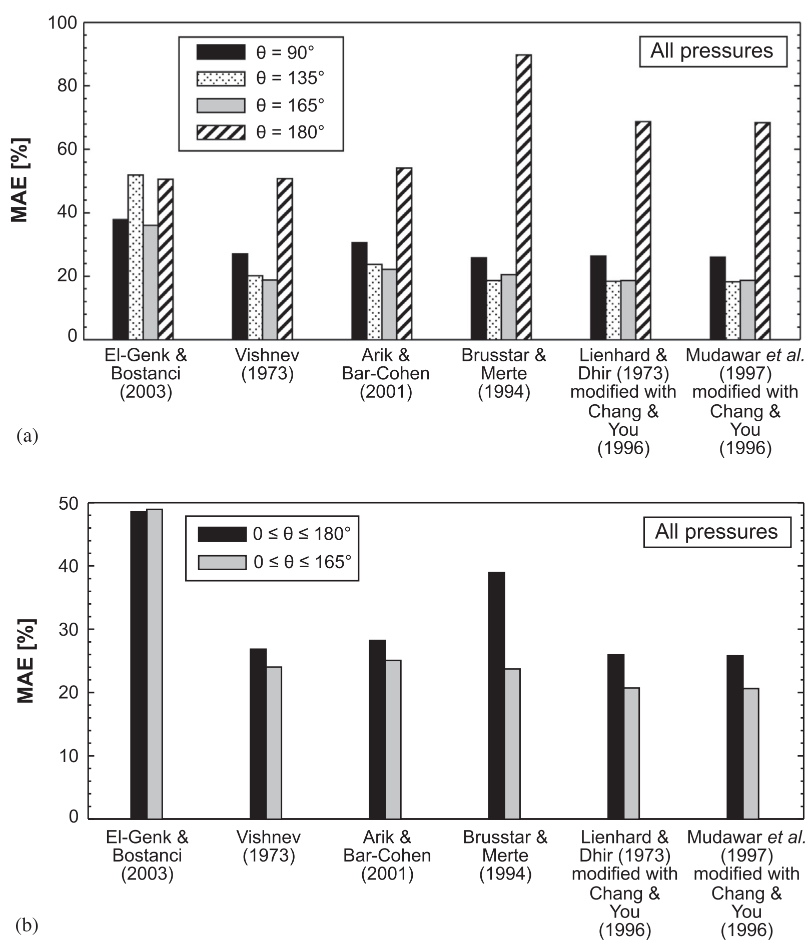

Fig. 11. (a) Distribution of MAE for all pressures and specific orientation angles, and (b) overall MAE for all pressures and different orientation angle ranges including $\theta = 0°$.

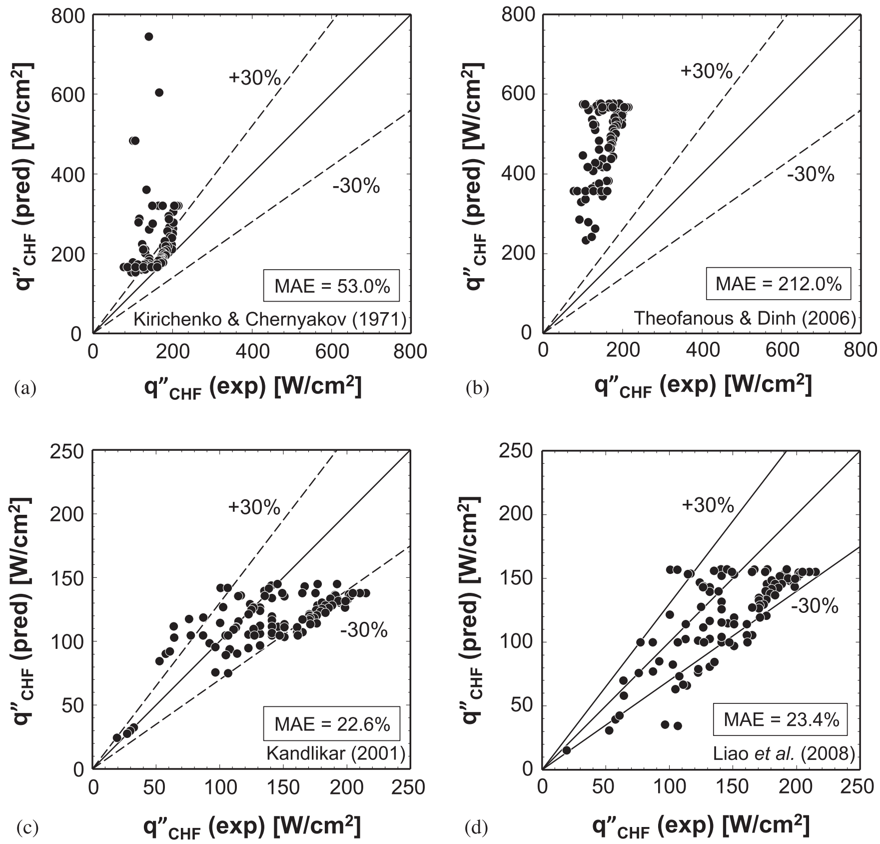

Fig. 13. Comparison of CHF data for all orientations with predictions of models or correlations accounting for contact angle: (a) Kirichenko and Chernyakov [39], (b) Theofanous and Dinh [26], (c) Kandlikar [40], and (d) Liao et al. [41].

Table 7
Comparison of individual CHF databases with predictions of models and correlations accounting for contact angle effects.

Database source	Fluid(s)	Mean absolute error [%]			
		Kirichenko & Chernyakov [39]	Theofanous & Dinh [26]	Kandlikar [40]	Liao et al. [41]
Kim et al. [48]	Water	50.5	223.7	22.5	21.9
Kim et al. [49]	Water	67.4	197.0	19.6	27.8
Kwark et al. [50]	Water	21.6	177.2	24.6	30.1
Ahn et al. [51]	Water	171.0	305.8	18.0	11.5
Saeidi & Alemrajabi [52]	Water	29.1	192.6	21.1	20.8
O'Hanley et al. [53]	Water	182.0	210.1	48.4	22.9
Park et al. [54]	Water	35.1	221.3	12.0	13.4
Liaw & Dhir [68]	R-113, water	–	–	19.1	55.0
Liao et al. [41]	Water	59.3	292.7	16.4	0.9
Wang & Dhir [74]	Water	–	–	20.8	36.7
Total		53.0	212.0	22.6	23.4

4.5. Recommended methods for predicting pool boiling CHF

After the assessment of 18 popular models and correlations used to predict pool boiling CHF against the present consolidated database, a set of seven methods with lowest MAEs are recommended for three different cases, as shown in Table 8.

For the horizontal, upward-facing orientation and entire pressure range, best predictions are achieved by the hydrodynamic instability model of Lienhard and Dhir [29,30] and interfacial lift-off model of Mudawar et al. [27].

For inclined orientations and atmospheric pressure, the new relations based on the Lienhard and Dhir model modified with the Chang and You correlation [38], Eq. (5a), and the Mudawar et al. model modified with the Chang and You correlation, Eq. (5b), along with the empirical correlation of Vishnev [34] provide the best predictions.

Finally, superior predictions for different orientation angles and contact angles in the range of $0° \leq \alpha \leq 90°$ are achieved by Kandlikar's model [40] and empirical correlation of Liao et al. [41]. It should also be mentioned that a large number of studies in the past two decades have been dedicated to enhancing CHF using a variety of surface modification techniques, a comprehensive review of which is now ongoing by the present authors. These techniques include nanoparticle deposition induced by nanofluid boiling [50], nanowire-coated surfaces [84], and surface anodization [85], in which improved surface wettability is a major contributor to

Table 8
Summary of methods for prediction of pool boiling CHF.

Author(s)	Relation	MAE [%]
Horizontal, upward-facing orientation		
Lienhard & Dhir [29,30]	$q''_{CHF} = 0.149\rho_g h_{fg}\left[\sigma g(\rho_f - \rho_g)/\rho_g^2\right]^{1/4}$	19.0
Mudawar et al. [27]	$q''_{CHF} = 0.151\rho_g h_{fg}\left[\sigma g(\rho_f - \rho_g)/\rho_g^2\right]^{1/4}$	19.1
Atmospheric pressure, all orientation angles		
Mudawar et al. model [27] modified with Chang & You correlation [38]	$q''_{CHF} = 0.151[1 - 0.0012\theta\tan(0.414\theta) - 0.122\sin(0.318\theta)] \times \rho_g h_{fg}\left[\sigma g(\rho_f - \rho_g)/\rho_g^2\right]^{1/4}$	23.3
Lienhard & Dhir model [29,30] modified with Chang & You correlation [38]	$q''_{CHF} = 0.149[1 - 0.0012\theta\tan(0.414\theta) - 0.122\sin(0.318\theta)] \times \rho_g h_{fg}\left[\sigma g(\rho_f - \rho_g)/\rho_g^2\right]^{1/4}$	23.8
Vishnev correlation [34]	$q''_{CHF} = 0.0125(190 - \theta)^{1/2}\rho_g h_{fg}\left[\sigma g(\rho_f - \rho_g)/\rho_g^2\right]^{1/4}$	25.5
All pressures and all orientation angles, with contact angles in the range of $0 \le \alpha \le 90°$		
Kandlikar [40]	$q''_{CHF} = \frac{1+\cos\alpha}{16}\left[\frac{2}{\pi} + \frac{\pi}{4}(1+\cos\alpha)\cos\theta\right]^{1/2} \times \rho_g h_{fg}\left[\sigma g(\rho_f - \rho_g)/\rho_g^2\right]^{1/4}$	22.6
Liao et al. [41]	$q''_{CHF} = 0.131\left[-0.73 + \frac{1.73}{1+10^{-0.021\times(185.4-\theta)}}\right]\left[1 + \frac{55-\alpha}{100}(0.56 - 0.0013\theta)\right] \times \rho_g h_{fg}\left[\sigma g(\rho_f - \rho_g)/\rho_g^2\right]^{1/4}$	23.4

the CHF enhancement. Thus, Kandlikar's model and the correlation of Liao et al. might contribute to the prediction of enhanced CHF resulting from these wettability effects.

4.6. Need for additional data and predictive methods

Despite the success of several available models at predicting the effects of pressure, surface orientation, and contact angle on pool boiling CHF, there is a need for consistent reduced gravity data to assess the ability of the same or improved tools in predicting the dependence of CHF on gravity. Overall, better success has been achieved in predicting reduced gravity CHF for flow boiling [86,87] than for pool boiling [88–90].

5. Concluding remarks

This paper is the second part of a two-part study on pool boiling CHF from flat surfaces. While the first part reviewed different CHF models and associated mechanisms and parametric trends, the present part was dedicated to assessment of CHF models and correlations. The assessment is based on a new consolidated CHF database that is amassed from 37 sources, and consists of 800 data points covering 14 working fluids, pressures from 0.0016 to 5.2 MPa, orientation angles from 0 to 180°, and contact angles from 0 to 113°. Key findings from this part can be summarized as follows:

(1) For the horizontal, upward-facing orientation, best predictions for the entire range of operating pressures are achieved with the modified hydrodynamic instability model of Lienhard and Dhir [29,30] and interfacial lift-off model of Mudawar et al. [27].
(2) For inclined surfaces, best predictions are achieved by modifying the models of Lienhard and Dhir, and Mudawar et al. with the CHF orientation correlation of Chang and You [38]. Higher predictive accuracy is achieved when data at or close to the horizontal, downward-facing orientation are excluded, which points to the need for more data and improved understanding of near-wall interfacial behavior for these orientations.
(3) CHF data reflecting contact angle effects are relatively sparse and limited to hydrophilic liquids. Overall, best predictions for contact angle effects are achieved with Kandlikar's model [40] and a correlation by Liao et al. [41].
(4) This paper is concluded with recommendations for most accurate models and correlations, segregated into three categories: (a) horizontal, upward-facing surfaces and all pressures, (b) tilted surfaces and atmospheric pressure alone, and (c) contact angle effects.

Conflict of interest

The authors declared that there is no conflict of interest.

Acknowledgement

Support of the National Natural Science Foundation of China under Grant No. 51506023 and the Fundamental Research Funds for Central Universities of Ministry of Education of China under Grant No. DUT17RC(4)22 is gratefully acknowledged.

References

[1] I. Mudawar, Assessment of high-heat-flux thermal management schemes, IEEE Trans. Compon. Packag. Technol. 24 (2001) 122–141.
[2] I. Mudawar, Recent advances in high-flux, two-phase thermal management, J. Therm. Sci. Eng. Appl. 5 (2013) 021012.
[3] T.J. LaClair, I. Mudawar, Thermal transients in a capillary evaporator prior to the initiation of boiling, Int. J. Heat Mass Transf. 43 (2000) 3937–3952.
[4] I. Mudawar, T.M. Anderson, Optimization of enhanced surfaces for high flux chip cooling by pool boiling, J. Electron. Packag. 115 (1993) 89–100.
[5] J.A. Shmerler, I. Mudawwar, Local heat transfer coefficient in wavy free-falling turbulent liquid films undergoing uniform sensible heating, Int. J. Heat Mass Transf. 31 (1988) 67–77.
[6] C.O. Gersey, I. Mudawar, Effects of heater length and orientation on the trigger mechanism for near-saturated flow boiling critical heat flux–I. Photographic study and statistical characterization of the near-wall interfacial features, Int. J. Heat Mass Transf. 38 (1995) 629–641.
[7] T.C. Willingham, I. Mudawar, Forced-convection boiling and critical heat flux from a linear array of discrete heat sources, Int. J. Heat Mass Transf. 35 (1992) 2879–2890.
[8] D.E. Maddox, I. Mudawar, Single-and two-phase convective heat transfer from smooth and enhanced microelectronic heat sources in a rectangular channel, J. Heat Transf. 101 (1989) 1045–1052.
[9] J. Lee, I. Mudawar, Critical heat flux for subcooled flow boiling in micro-channel heat sinks, Int. J. Heat Mass Transf. 52 (2009) 3341–3352.
[10] J. Lee, I. Mudawar, Fluid flow and heat transfer characteristics of low temperature two-phase micro-channel heat sinks–Part 1: Experimental methods and flow visualization results, Int. J. Heat Mass Transf. 51 (2008) 4315–4326.
[11] D.D. Hall, I. Mudawar, Ultra-high critical heat flux (CHF) for subcooled water flow boiling–II: high-CHF database and design equations, Int. J. Heat Mass Transf. 42 (1999) 1429–1456.
[12] D.C. Wadsworth, I. Mudawar, Enhancement of single-phase heat transfer and critical heat flux from an ultra-high-flux simulated microelectronic heat source to a rectangular impinging jet of dielectric liquid, J. Heat Transf. 114 (1992) 764–768.

[13] M.E. Johns, I. Mudawar, An ultra-high power two-phase jet-impingement avionic clamshell module, J. Electron. Packag. 118 (1996) 264–270.
[14] S. Mukherjee, I. Mudawar, Smart pumpless loop for micro-channel electronic cooling using flat and enhanced surfaces, IEEE Trans. Compon. Packag. Technol. 26 (2003) 99–109.
[15] J.D. Bernardin, I. Mudawar, A Leidenfrost point model for impinging droplets and sprays, J. Heat Transf. 126 (2004) 272–278.
[16] M. Visaria, I. Mudawar, Effects of high subcooling on two-phase spray cooling and critical heat flux, Int. J. Heat Mass Transf. 51 (2008) 5269–5278.
[17] I. Mudawar, D. Bharathan, K. Kelly, S. Narumanchi, Two-phase spray cooling of hybrid vehicle electronics, IEEE Trans. Compon. Packag. Technol. 32 (2009) 501–512.
[18] M.K. Sung, I. Mudawar, Experimental and numerical investigation of single-phase heat transfer using a hybrid jet-impingement/micro-channel cooling scheme, Int. J. Heat Mass Transf. 49 (2006) 682–694.
[19] G. Liang, I. Mudawar, Pool boiling critical heat flux (CHF)–Part 1: Review of mechanisms, models, and correlations, Int. J. Heat Mass Transf. 117 (2017) 1352–1367.
[20] W.M. Rohsenow, P. Griffith, Correlation of maximum heat transfer data for boiling of saturated liquids, Chem. Eng. Prog. Symp. Ser. 52 (1955) 47–49.
[21] N. Zuber, On the stability of boiling heat transfer, Trans. ASME 80 (1958) 711–720.
[22] N. Zuber, Hydrodynamic aspects of boiling heat transfer, PhD Dissertation, University of California, Los Angeles, USA, 1959.
[23] N. Zuber, M. Tribus, J.W. Westwater, The hydrodynamic crisis in pool boiling of saturated and subcooled liquids, in: International Developments in Heat Transfer: Proc. Int. Heat Transfer Conf., Boulder, USA, 1961, pp. 230–236.
[24] Y. Haramura, Y. Katto, A new hydrodynamic model of critical heat flux, applicable widely to both pool and forced convection boiling on submerged bodies in saturated liquids, Int. J. Heat Mass Transf. 26 (1983) 389–399.
[25] V.V. Yagov, Is a crisis in pool boiling actually a hydrodynamic phenomenon?, Int J. Heat Mass Transf. 73 (2014) 265–273.
[26] T.G. Theofanous, T.-N. Dinh, High heat flux boiling and burnout as microphysical phenomena: mounting evidence and opportunities, Multiph. Sci. Technol. 18 (2006) 251–276.
[27] I. Mudawar, A.H. Howard, C.O. Gersey, An analytical model for near-saturated pool boiling critical heat flux on vertical surfaces, Int. J. Heat Mass Transf. 40 (1997) 2327–2339.
[28] S.S. Kutateladze, On the transition to film boiling under natural convection, Kotloturbostroenie 3 (1948) 10–12.
[29] J.H. Lienhard, V.K. Dhir, Extended hydrodynamic theory of the peak and minimum pool boiling heat fluxes, NASA Report No. NASA CR-2270, University of Kentucky, Lexington, 1973.
[30] J.H. Lienhard, V.K. Dhir, Hydrodynamic prediction of peak pool-boiling heat fluxes from finite bodies, J. Heat Transf. 95 (1973) 152–158.
[31] L. Wang, Y. Li, F. Zhang, F. Xie, Y. Ma, Correlations for calculating heat transfer of hydrogen pool boiling, Int. J. Hydrogen Energy 41 (2016) 17118–17131.
[32] C.-K. Guan, J.F. Klausner, R. Mei, A new mechanistic model for pool boiling CHF on horizontal surfaces, Int. J. Heat Mass Transf. 54 (2011) 3960–3969.
[33] M.S. El-Genk, H. Bostanci, Saturation boiling of HFE-7100 from a copper surface, simulating a microelectronic chip, Int. J. Heat Mass Transf. 46 (2003) 1841–1854.
[34] I.P. Vishnev, Effect of orienting the hot surface with respect to the gravitational field on the critical nucleate boiling of a liquid, J. Eng. Phys. Thermophys. 24 (1973) 43–48.
[35] M. Arik, A. Bar-Cohen, Ebullient cooling of integrated circuits by Novec fluids, in: Proc. Pacific Rim Int. Intersociety Electronic Packaging Conf., Hawaii, USA, 2001.
[36] M.J. Brusstar, H. Merte, Effects of heater surface orientation on the critical heat flux–II. A model for pool and forced convection subcooled boiling, Int. J. Heat Mass Transf. 40 (1997) 4021–4030.
[37] M.J. Brusstar, H. Merte Jr., Effects of buoyancy on the critical heat flux in forced convection, J. Thermophys. Heat Transf. 8 (1994) 322–328.
[38] J.Y. Chang, S.M. You, Heater orientation effects on pool boiling of micro-porous-enhanced surfaces in saturated FC-72, J. Heat Transf. 118 (1996) 937–943.
[39] Y.A. Kirichenko, P.S. Chernyakov, Determination of the first critical thermal flux on flat heaters, J. Eng. Phys. Thermophys. 20 (1971) 699–703.
[40] S.G. Kandlikar, A theoretical model to predict pool boiling CHF incorporating effects of contact angle and orientation, J. Heat Transf. 123 (2001) 1071–1079.
[41] L. Liao, R. Bao, Z. Liu, Compositive effects of orientation and contact angle on critical heat flux in pool boiling of water, Heat Mass Transf. 44 (2008) 1447–1453.
[42] S.J. Kim, I.C. Bang, J. Buongiorno, L.W. Hu, Surface wettability change during pool boiling of nanofluids and its effect on critical heat flux, Int. J. Heat Mass Transf. 50 (2007) 4105–4116.
[43] W. Bailey, E. Young, C. Beduz, Y. Yang, Pool boiling study on candidature of pentane, methanol and water for near room temperature cooling, in: Thermal and Thermomechanical Phenomena in Electronics Systems, IEEE, San Diego, USA, 2006, pp. 599–603.
[44] C.-K. Guan, B. Bon, J. Klausner, R. Mei, Comparison of CHF enhancement on microstructured surfaces with a predictive model, Heat Transf. Eng. 35 (2014) 452–460.
[45] D.N. Lyon, P.G. Kosky, B.N. Harman, Nucleate boiling heat transfer coefficients and peak nucleate boiling fluxes for pure liquid nitrogen and oxygen on horizontal platinum surfaces from below 0.5 atmosphere to the critical pressures, in: K.D. Timmerhaus (Ed.), Advances in Cryogenic Engineering, Springer, New York, 1964, pp. 77–87.
[46] T.G. Theofanous, T.-N. Dinh, J.P. Tu, A.T. Dinh, The boiling crisis phenomenon: Part II: dryout dynamics and burnout, Exp. Therm. Fluid Sci. 26 (2002) 793–810.
[47] D.A. Labuntsov, V.V. Jagov, A.K. Gorodov, Critical heat fluxes in boiling at low pressure region, in: Proc. 6th Int. Heat Transfer Conf., Toronto, Canada, 1978, pp. 221–225.
[48] J. Kim, S. Jun, R. Laksnarain, S.M. You, Effect of surface roughness on pool boiling heat transfer at a heated surface having moderate wettability, Int. J. Heat Mass Transf. 101 (2016) 992–1002.
[49] J. Kim, S. Jun, S.M. You, Effect of surface roughness on pool boiling heat transfer of water on a superhydrophilic aluminum surface, ASME 2016 Int. Mechanical Engineering Congress and Exposition, ASME, Phoenix, USA, 2016.
[50] S.M. Kwark, G. Moreno, R. Kumar, H. Moon, S.M. You, Nanocoating characterization in pool boiling heat transfer of pure water, Int. J. Heat Mass Transf. 53 (2010) 4579–4587.
[51] H.S. Ahn, C. Lee, H. Kim, H. Jo, S. Kang, J. Kim, J. Shin, M.H. Kim, Pool boiling CHF enhancement by micro/nanoscale modification of zircaloy-4 surface, Nucl. Eng. Des. 240 (2010) 3350–3360.
[52] D. Saeidi, A.A. Alemrajabi, Experimental investigation of pool boiling heat transfer and critical heat flux of nanostructured surfaces, Int. J. Heat Mass Transf. 60 (2013) 440–449.
[53] H. O'Hanley, C. Coyle, J. Buongiorno, T. McKrell, L.-W. Hu, M. Rubner, R. Cohen, Separate effects of surface roughness, wettability, and porosity on the boiling critical heat flux, Appl. Phys. Lett. 103 (2013) 024102.
[54] S.C. Park, J.M. Kim, T. Kim, M.H. Kim, H.S. Ahn, Boiling characteristics on a serpentine-like geometry thin-film platinum heater under pool boiling, Int. J. Heat Mass Transf. 95 (2016) 214–223.
[55] Z. Guo, M.S. El-Genk, An experimental study of saturated pool boiling from downward facing and inclined surfaces, Int. J. Heat Mass Transf. 35 (1992) 2109–2117.
[56] C. Beduz, R.G. Scurlock, A.J. Sousa, Angular dependence of boiling heat transfer mechanisms in liquid nitrogen, in: R.W. Fast (Ed.), Advances in Cryogenic Engineering, Springer, New York, 1988, pp. 363–370.
[57] S. Nishio, G.R. Chandratilleke, Steady-state pool boiling heat transfer to saturated liquid helium at atmospheric pressure, JSME Int. J. Ser. II 32 (1989) 639–645.
[58] Y. Katto, S. Yokoya, M. Yasunaka, Mechanism of boiling crisis and transition boiling in pool boiling, 4th Int. Heat Transfer Conf., Begel House Inc., Paris-Versailles, France, 1970.
[59] H. Sakashita, A. Ono, J. Nyui, Critical heat flux and near-wall boiling behaviors in saturated and subcooled pool boiling on vertical and inclined surfaces, J. Nucl. Sci. Technol. 46 (2009) 1038–1048.
[60] H. Sakashita, Critical heat flux on a vertical surface in saturated pool boiling at high pressures, J. Therm. Sci. Technol. 11 (2016) 16–00264.
[61] M. Monde, H. Kusuda, H. Uehara, Critical heat flux during natural convective boiling in vertical rectangular channels submerged in saturated liquid, J. Heat Transf. 104 (1982) 300–303.
[62] A.H. Howard, I. Mudawar, Orientation effects on pool boiling critical heat flux (CHF) and modeling of CHF for near-vertical surfaces, Int. J. Heat Mass Transf. 42 (1999) 1665–1688.
[63] S.J. Reed, I. Mudawar, Enhancement of boiling heat transfer using highly wetting liquids with pressed-on fins at low contact forces, Int. J. Heat Mass Transf. 40 (1997) 2379–2392.
[64] M. Jergel, R. Stevenson, Static heat transfer to liquid helium in open pools and narrow channels, Int. J. Heat Mass Transf. 14 (1971) 2099–2107.
[65] L. Bewilogua, R. Knöner, H. Vinzelberg, Heat transfer in cryogenic liquids under pressure, Cryogenics 15 (1975) 121–125.
[66] V.I. Deev, V.E. Keilin, I.A. Kovalev, A.K. Kondratenko, V.I. Petrovichev, Nucleate and film pool boiling heat transfer to saturated liquid helium, Cryogenics 17 (1977) 557–562.
[67] I.I. Gogonin, S.S. Kutateladze, Critical heat flux as a function of heater size for a liquid boiling in a large enclosure, J. Eng. Phys. 33 (1977) 1286–1289.
[68] S.P. Liaw, V.K. Dhir, Effect of surface wettability on transition boiling heat transfer from a vertical surface, in: Proc. 8th Int. Heat Transfer Conf., San Francisco, USA, 1986, pp. 2031–2036.
[69] A. Priarone, Effect of surface orientation on nucleate boiling and critical heat flux of dielectric fluids, Int. J. Therm. Sci. 44 (2005) 822–831.
[70] D. Zhong, J.a. Meng, Z. Li, Z. Guo, Critical heat flux for downward-facing saturated pool boiling on pin fin surfaces, Int. J. Heat Mass Transf. 87 (2015) 201–211.
[71] Y.H. Kim, S.J. Kim, J.J. Kim, S.W. Noh, K.Y. Suh, J.L. Rempe, F.B. Cheung, S.B. Kim, Visualization of boiling phenomena in inclined rectangular gap, Int. J. Multiph. Flow 31 (2005) 618–642.
[72] S.M. Kwark, M. Amaya, R. Kumar, G. Moreno, S.M. You, Effects of pressure, orientation, and heater size on pool boiling of water with nanocoated heaters, Int. J. Heat Mass Transf. 53 (2010) 5199–5208.
[73] K.N. Rainey, S.M. You, Effects of heater size and orientation on pool boiling heat transfer from microporous coated surfaces, Int. J. Heat Mass Transf. 44 (2001) 2589–2599.
[74] C.H. Wang, V.K. Dhir, Effect of surface wettability on active nucleation site density during pool boiling of water on a vertical surface, J. Heat Transf. 115 (1993) 659–669.
[75] M. Maracy, R.H.S. Winterton, Hysteresis and contact angle effects in transition pool boiling of water, Int. J. Heat Mass Transf. 31 (1988) 1443–1449.

[76] S.H. Yang, W.-P. Baek, S.H. Chang, Pool-boiling critical heat flux of water on small plates: effects of surface orientation and size, Int. Commun. Heat Mass Transfer 24 (1997) 1093–1102.

[77] A.A. Watwe, A. Bar-Cohen, Modeling of conduction effects on pool boiling CHF of dielectric liquids, in: Proc. 32nd National Heat Transfer Conf., Baltimore, USA, 1997.

[78] I. Golobič, A.E. Bergles, Effects of heater-side factors on the saturated pool boiling critical heat flux, Exp. Therm. Fluid Sci. 15 (1997) 43–51.

[79] H. Sakashita, A. Ono, Boiling behaviors and critical heat flux on a horizontal plate in saturated pool boiling of water at high pressures, Int. J. Heat Mass Transf. 52 (2009) 744–750.

[80] E.W. Lemmon, M.L. Huber, M.O. McLinden, NIST Reference Fluid Thermodynamic and Transport Properties–REFPROP Version 8.0, NIST, Gaithersburg, USA, 2007.

[81] D.N. Lyon, Peak nucleate-boiling heat fluxes and nucleate-boiling heat-transfer coefficients for liquid N_2, liquid O_2 and their mixtures in pool boiling at atmospheric pressure, Int. J. Heat Mass Transf. 7 (1964) 1097–1116.

[82] M. El-Genk, H. Bostanci, Combined effects of subcooling and surface orientation on pool boiling of HFE-7100 from a simulated electronic chip, Exp. Heat Transf. 16 (2003) 281–301.

[83] M.J. Brusstar, H. Merte, R.B. Keller, B.J. Kirby, Effects of heater surface orientation on the critical heat flux–I. An experimental evaluation of models for subcooled pool boiling, Int. J. Heat Mass Transf. 40 (1997) 4007–4019.

[84] R. Chen, M.-C. Lu, V. Srinivasan, Z. Wang, H.H. Cho, A. Majumdar, Nanowires for enhanced boiling heat transfer, Nano Lett. 9 (2009) 548–553.

[85] H.S. Ahn, H.J. Jo, S.H. Kang, M.H. Kim, Effect of liquid spreading due to nano/microstructures on the critical heat flux during pool boiling, Appl. Phys. Lett. 98 (2011) 071908.

[86] H. Zhang, I. Mudawar, M.M. Hasan, Flow boiling CHF in microgravity, Int. J. Heat Mass Transf. 48 (2005) 3107–3118.

[87] H. Zhang, I. Mudawar, M.M. Hasan, Experimental assessment of the effects of body force, surface tension force, and inertia on flow boiling CHF, Int. J. Heat Mass Transf. 45 (2002) 4079–4095.

[88] C. Konishi, I. Mudawar, Review of flow boiling and critical heat flux in microgravity, Int. J. Heat Mass Transf. 80 (2015) 469–493.

[89] H. Merte, J.A. Clark, Pool boiling in an accelerating system, J. Heat Transf. 83 (1961) 233–242.

[90] H. Merte, J.A. Clark, Boiling heat transfer with cryogenic fluids at standard, fractional, and near-zero gravity, J. Heat Transf. 86 (1964) 351–358.